On the measurement of the proton structure at small Q^2

J Blümlein†, G Levman‡ and H Spiesberger§

† DESY, Institut für Hochenergiephysik IfH, Zeuthen, Federal Republic of Germany
‡ Department of Physics, University of Toronto, Canada
§ Fakultät für Physik, Universität Bielefeld, Federal Republic of Germany

Abstract. Large-angle radiative scattering at HERA, $ep \to e\gamma X$, can be used for a measurement of the low-Q^2 behaviour of proton structure functions. The measurement can be interpreted as probing the photon density of the proton through virtual Compton scattering.

1. Introduction

Electromagnetic radiative corrections to neutral-current deep-inelastic scattering at HERA are large [1] if the kinematical variables are measured from the scattered lepton. At small x and large y, the cross section for bremsstrahlung $ep \to e\gamma X$ may reach the magnitude of the Born cross section of the non-radiative process $ep \to eX$. These large corrections make the analysis of experimental data, which aims at presenting measured values in terms of the Born cross section, rather difficult in the case of a lepton-inclusive measurement. However, radiative events are interesting in their own right because they provide experimenters with additional possibilities for making physics measurements.

Wide-angle bremsstrahlung has been reviewed both theoretically and experimentally by Grammer and Sullivan [2]. More recently, experiments have measured wide-angle bremsstrahlung as checks of radiative correction calculations [3] and in search of radiation from quarks [4]. At HERA the experiments use elastic bremsstrahlung to measure luminosity and to monitor the electron beam. A further example of the use of radiative deep-inelastic scattering was discussed in [5]. There it was shown that the emission of photons collinear with the initial-state electron leads to a shift in the effective beam energy which can be used for a measurement of the longitudinal structure function $F_L(x, Q^2)$.

In the calculation of radiative corrections to neutral-current deep-inelastic scattering in the leading logarithmic approximation [6–8], one may decompose the total correction into parts associated not only with initial- and final-state radiation, but also a part associated with nearly collinear emission of the exchanged photon from quarks or from the proton, the Compton peak†. In the present work, we will argue that the Compton peak can be used for a determination of the proton's structure functions. This was first pointed out in [10].

The cross section associated with the Compton peak is large, despite the fact that it contains an additional factor $\alpha = 1/137$ compared to the tree-level cross section for $ep \to eX$. This follows since the emission of a large-p_T photon can lead to a reduction of the true momentum transfer with respect to that measured from the scattered electron; $Q_l^2 = -(l - l')^2$ is shifted to $Q_h^2 = -(l - l' - k)^2$ and Q_h^2 can become of the order of the proton mass squared, or even smaller, if the photon's transverse momentum is balanced by

† A similar decomposition of the QED radiative corrections was carried out in the peaking-approximation in the early work by Mo and Tsai [9]. There, the Compton peak was mentioned first as the 'third peak'.

that of the electron. The reduction in Q^2 and the corresponding increase of the cross section compensates to a large extent for the smallness of the additional factor α. Thus large-angle radiative scattering with $p_T^e = p_T^\gamma$ can be expected to provide a tool to investigate the small-Q^2 behaviour of the proton structure functions at HERA in the *small-x* range

The experimental signature of Compton peak events is an electron–photon pair, which is nearly balanced in p_T, and low (if any) visible hadronic activity. Because most of the hadronic activity is lost down the beam pipe, experimental selection criteria remove these events from the deep-inelastic neutral-current scattering sample. As a result, Compton events do not contribute to radiative corrections. However, since they are easily recognized, and do not contain much background from other reactions, a measurement of the Compton contribution to radiative events is feasible at HERA [11].

2. The Compton peak

We consider the scattering of electrons of momentum l off protons with 4-momentum p. Events with a scattered electron of momentum l' can be seen in the detector if the transverse component of l', l'_T, is large enough. These events have large $Q_l^2 = -(l - l')^2$. If a photon of momentum k is emitted at the lepton vertex, the momentum squared which is transferred to the hadronic system is $Q_h^2 = -(l - l' - k)^2$. The lower kinematical limit for Q_h^2 is

$$Q^2_{h,\min} = \frac{x_l^2 m_p^2}{1 - x_l} \tag{1}$$

where m_p denotes the proton mass and

$$x_l = \frac{Q_l^2}{2p \cdot (l - l')}. \tag{2}$$

When this lower limit is reached the photon energy E_γ and its scattering angle θ_γ are related to the leptonic variables Q_l^2, x_l and $y_l = Q_l^2/(x_l s)$ ($s = (l + p)^2$, neglecting the masses of the electron and of the proton) by

$$E_\gamma = y_l E_e + x_l(1 - y_l) E_p \tag{3}$$

$$\cos\theta_\gamma = \frac{y_l E_e - x_l(1 - y_l) E_p}{y_l E_e + x_l(1 - y_l) E_p} \tag{4}$$

where E_e and E_p denote the energies of the initial electron and proton, respectively. Thus, for $Q_h^2 = Q^2_{h,\min}$, the transverse momentum of the photon

$$k_T = E_\gamma \sin\theta_\gamma = 2\sqrt{x_l y_l (1 - y_l) E_e E_p} \tag{5}$$

balances the transverse momentum of the scattered electron

$$l'_T = k_T. \tag{6}$$

Events of the Compton peak are characterized by $Q_h^2 \simeq 0$. They are thus events where the final-state electron and the photon are produced at large transverse momenta which are nearly balanced. Since the mass of the hadronic final state is related to the momentum

transfer by $W^2 = p_X^2 = m_p^2 + Q_h^2(1 - x_h)/x_h$ with $x_h = Q_h^2/[2p \cdot (l - l' - k)]$, $0 \leqslant x_h \leqslant 1$, it is clear that these events will most probably have a small hadronic mass and the process will be dominated by (quasi-)elastic and resonant electron–proton scattering: $ep \to ep\gamma$ and $ep \to e\gamma N^* \to e\gamma N\pi$ with $N\pi = p\pi^0$ or $n\pi^+$.

If one is interested in the deep-inelastic contribution to $ep \to e\gamma X$ one will have to impose a minimum cut on the hadronic mass $W \gtrsim 2\,\mathrm{GeV}$ to exclude both the quasi-elastic and resonant contributions. In principle, the hadronic mass may be calculated from the measured kinematical information using

$$W^2 = (l - l' - k + p)^2 = s - 2(l + p)(l' + k) + (l' + k)^2. \tag{7}$$

However, due to a cancellation of large numbers in (7) the measurement error of W^2 is large. On the other hand, in the case of quasi-elastic and resonant production the hadronic final state should contain only a single fast proton or a fast nucleon and pion. An experiment with a leading-particle spectrometer can tag events with protons scattered at $x_F < 1$. With a hadron calorimeter at zero degrees, an experiment can also identify inelastic events with produced neutrons. Moreover, the quasi-elastic and resonant contributions to the Compton peak may be well simulated by Monte Carlo calculations [12, 13], since the corresponding electromagnetic form factors $F_i(Q_h^2)$ are known from other experiments, and simple parametrizations for their Q^2 behaviour exist (see, for example, [14]).

At small Q_h^2, the process is dominated by photon exchange. The Z exchange amplitude is suppressed by $\sim Q_h^2/M_Z^2$ and we may safely neglect it in the following. The cross section for radiative electron–proton scattering $ep \to e\gamma X$ is well known and can be derived assuming one-photon exchange in a model-independent way using the structure functions F_2 and $F_L = F_2 - 2xF_1$ (see, for example, [9, 15]). In the limit of small Q_h^2, the result is

$$\left.\frac{d^2\sigma}{dx_l\,dy_l}\right|^C = \frac{\alpha^3}{x_l s}\frac{1 + (1 - y_l)^2}{1 - y_l} \times \int_{x_l}^1 dz \int_{Q_{h,\min}^2}^{Q_l^2} \frac{dQ_h^2}{Q_h^2}\frac{z}{x_l}\left[\frac{1 + (1 - z)^2}{z^2}F_2\left(\frac{x_l}{z}, Q_h^2\right) - F_L\left(\frac{x_l}{z}, Q_h^2\right)\right]. \tag{8}$$

Note that, in general, the structure functions $F_{2,L}(x, Q^2)$ cannot be represented in terms of parton densities since Q_h^2 can become very small and perturbative QCD is no longer applicable.

Equation (8) can be written as a convolution of a probability distribution to find a photon inside the proton, $D_{\gamma/p}(z)$, and the cross section for Compton scattering of an electron $e\gamma \to e\gamma$:

$$\left.\frac{d^2\sigma}{dx_l\,dy_l}\right|^C = \int_0^1 \frac{dz}{z} D_{\gamma/p}(z, Q_l^2)\left.\frac{d^2\hat{\sigma}(e\gamma \to e\gamma)}{d\hat{x}\,dy_l}\right|_{\hat{s}=zs,\ \hat{x}=x_l/z} \tag{9}$$

with

$$\frac{d^2\hat{\sigma}(e\gamma \to e\gamma)}{d\hat{x}\,dy_l} = \frac{2\pi\alpha^2}{\hat{s}}\frac{1 + (1 - y_l)^2}{1 - y_l}\delta(1 - \hat{x}) \tag{10}$$

and

$$D_{\gamma/p}(x_l, Q_l^2) = \frac{\alpha}{2\pi}\int_{x_l}^1 dz \int_{Q_{h,\min}^2}^{Q_l^2} \frac{dQ_h^2}{Q_h^2}\frac{z}{x_l}\left[\frac{1 + (1 - z)^2}{z^2}F_2\left(\frac{x_l}{z}, Q_h^2\right) - F_L\left(\frac{x_l}{z}, Q_h^2\right)\right]. \tag{11}$$

It is instructive to consider the case where Q_h^2 is still of the order of a few GeV^2 and the parton model is valid. Inserting $F_L = 0$ (according to the Callan–Gross relation) and

$$F_2(x_h, Q_h^2) = x_h \sum_{f,\bar{f}} e_f^2 P_{q_f/p}(x_h, Q_h^2) \tag{12}$$

where $P_{q_f/p}$ are the parton distribution functions, one finds

$$D_{\gamma/p}(x_l, Q_l^2) = \frac{\alpha}{2\pi} \sum_{f,\bar{f}} \int_{Q_0^2}^{Q_l^2} \frac{dQ_h^2}{Q_h^2} \int_{x_l}^{1} \frac{dz}{z} P_{\gamma/q_f}(z, Q_h^2) \sum_{f,\bar{f}} e_f^2 P_{q_f/p}(x_l/z, Q_h^2) \tag{13}$$

with $Q_0^2 \gtrsim 2\,GeV^2$, and

$$P_{\gamma/q_f}(z) = \frac{1 + (1-z)^2}{z} \tag{14}$$

is the lowest-order Altarelli–Parisi splitting function for the transition $q_f \to \gamma$. Thus, the probability to find a photon inside the proton is a convolution of the probabilities to find first a quark inside the proton and then a photon inside the quark.

Equation (8) is the result of a collinear approximation where the exchanged photon is assumed to be emitted collinear with the incoming beams. It describes the leading logarithm $\ln Q^2/Q^2_{h,min} \simeq \ln Q^2/(x_l^2 m_p^2)$ which is needed in addition to the initial- and final-state collinear logarithms $\simeq \ln Q^2/m_e^2$ to describe the complete radiative corrections to $ep \to eX$.

In order to obtain an estimate of the cross section for Compton events expected at HERA one has to use a realistic parametrization of the structure functions $F_l(x, Q^2)$ over the full range of x and Q^2. We are interested in the region of phase space which is larger than that encompassed by any one parametrization. In particular, Q^2 and x can be small, outside the region of validity of the standard parametrizations of the deep-inelastic proton structure functions. In addition, if the structure function parametrizations are extrapolated to $Q^2 \to 0$, they do not satisfy the constraint that the structure functions must vanish in this limit as a consequence of gauge invariance. Clearly, the small-Q^2 behaviour is governed by non-perturbative effects, and cannot be described by perturbative QCD. One simple possibility is to use one of the standard parametrizations of parton distribution functions and to enforce the vanishing of F_2 for $Q^2 \to 0$ by a global suppression factor, such as [16] $S = [1 - \exp(-aQ^2)]$ with $a = 3.37\,GeV^{-2}$. In figure 1 the differential cross section as obtained from (8) is shown as a function of y_l for several values of x_l in the small-x_l range. Here we assumed $F_L = 0$, and parametrized $F_2(x, Q^2)$ using the recent distribution D'_- [17] in the DIS scheme for $Q^2 \geqslant 5\,GeV^2$. For lower Q^2 values the distributions were taken at $Q^2 = 5\,GeV^2$ and multiplied by S. The result is in accord with earlier calculations (see [7, 10]).

Various other parametrizations of the behaviour at small Q^2, in particular for F_2, are in use, which are partly motivated by phenomenological ansätze or measurements; however, they are valid only at larger values of x. A summary of the current parametrizations is given in [18]. For the Monte Carlo study to be discussed below we have chosen to piece together different structure function parametrizations. For $Q^2 < 6\,GeV^2$ and $W^2 < 4\,GeV^2$ we use the parametrization of Brasse [19]; for $Q^2 < 6\,GeV^2$ and $W^2 > 4\,GeV^2$ that of Stein [20]. For large values of Q^2 one of the standard deep-inelastic parametrizations can be used. We have chosen HMRSB [21] as an example. Our basic conclusions do not change significantly if we vary either the deep-inelastic structure function parametrization, or use a suppression factor rather than piecing together different structure function sets.

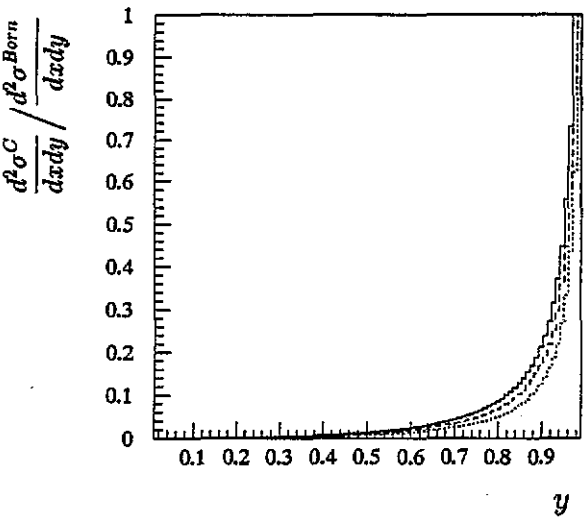

Figure 1. Differential Compton cross section (8) as a function of y_l for $x_l = 10^{-4}$ (dotted curve), 10^{-3} (broken curve), and 10^{-2} (full curve).

3. Monte Carlo simulation

In order to study the event characteristics of virtual Compton scattering at HERA we have used the Monte Carlo event generator HERACLES [12]. In the program the radiative cross section is divided into three channels. These channels correspond to the three peaks in the leading logarithm approximation to the full $\mathcal{O}(\alpha)$ calculation: initial- and final-state radiation and Compton radiation. It should be kept in mind that this division is not a division of the photon phase space and that tails of one channel appear in the kinematical regime of the others. In addition only the sum of all three channels correctly gives a gauge-invariant result.

In the kinematical limit of virtual Compton scattering hadronization schemes based on the quark model are invalid. In order to study the hadronic final state we model it as a hadronic cluster with the quantum numbers of the proton. We use the cluster decay model of the program HERWIG [22] to determine the decay products of the cluster.

We have generated events from all three channels in order to study the effects of kinematical cuts and of detector geometry. To a good approximation these effects are the same for the two detectors, ZEUS [23] and H1 [24], at HERA. Effects due to the finite resolution of detectors have not been included.

We have studied the kinematical range $10^{-4} < x_l < 0.5$, $0.01 < y_l < 0.99$ and $Q_l^2 > 4\,\mathrm{GeV}^2$. In this range the total radiative cross section for $E_\gamma > 1\,\mathrm{GeV}$ is 39 nb. The individual contributions from the three channels of HERACLES are 63% from initial-state radiation, 34% from final-state radiation, and 3% Compton events. We are interested in the kinematical regime where both the electron and photon have large energies and balance transverse momentum. The particles must be produced at large angles; otherwise they will be lost down the beam pipe. Accordingly, we require that E_e, $E_\gamma > 5\,\mathrm{GeV}$ and that the scattering angles satisfy θ_e, $\theta_\gamma > 10°$. The electron and photon are detected calorimetrically, and in order to ensure that the two showers are resolved and well measured we require, in addition, that the opening angle between them be relatively large, $\theta_{e\gamma} > 10°$. Finally, in order to select events in which the electron and photon balance transverse momentum we require that the missing transverse momentum satisfies $p_T^2 \leqslant 7.5\,\mathrm{GeV}^2$. The effect of these requirements can be summarized briefly as follows. The requirement that both the electron and the photon be produced at large angles with respect to the beam eliminates a large number of events, but suppresses most significantly initial-state radiative events

relative to final-state and Compton events. Then, the insistence on a large opening angle produces a sample composed of approximately an equal number of events from each of the three channels. The minimum energy requirement does not change this result. Finally, the requirement of transverse momentum balance leaves a sample of events of which 96% are Compton events, representing 7% of the original sample of Compton events.

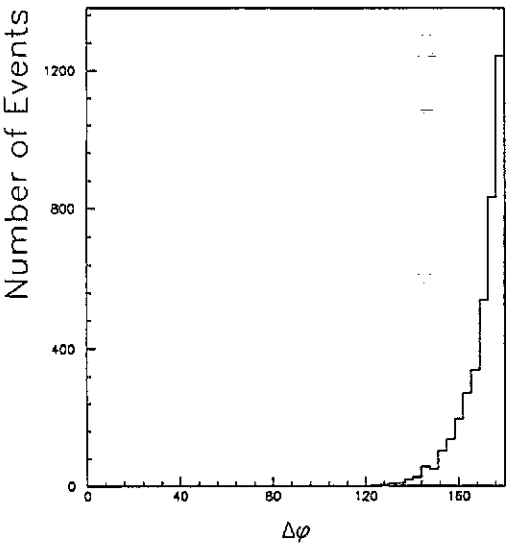

Figure 2. The difference in azimuth of the photon and electron for accepted Compton events.

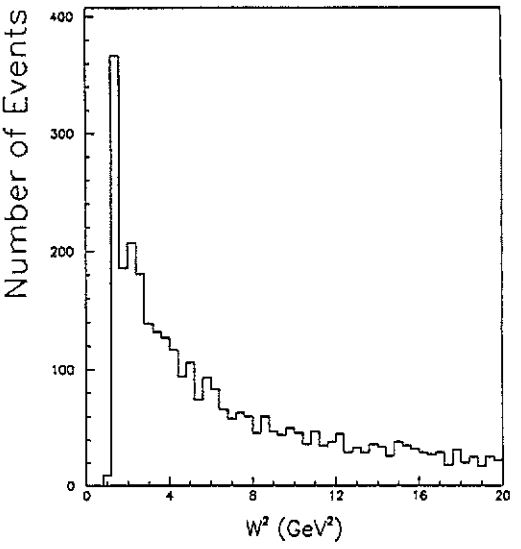

Figure 3. The hadronic mass distribution W^2 for accepted Compton events.

The difference between the azimuthal angle of the electron and the photon for the accepted Compton events is shown in figure 2. Since the two particles balance p_T they recoil nearly back-to-back. Two such isolated electromagnetic showers will form a very clean tag of the Compton events. The signature is especially striking since hadronic energy accompanying the electron and photon is small. Figure 3 shows the hadronic mass W^2 for the tagged events. The distribution peaks at the pπ threshold and falls rapidly. Because of the large boost from the laboratory to the rest frame of the fragmenting proton, most often the fragments of the proton are lost down the beam pipe. The cluster decay model of HERWIG predicts that this is the case over 90% of the time. Moreover, even if hadronic energy is caught by the calorimeter the amount is likely to be small ($\leqslant 5$ GeV), and deposited close to the proton direction (in the forward calorimeter of the experiments). Information on the hadronic final state is best obtained using a leading proton spectrometer and forward neutron calorimeter. These devices are presently being implemented in the ZEUS detector. In contrast to the hadronic final state, the photon and electron appear at small angles with respect to the electron direction, in the rear calorimeters. In recapitulation, the signature of the Compton events is two isolated back-to-back energetic electromagnetic showers, accompanied by little or no hadronic activity.

The momentum fraction carried by the exchanged photon is given by x_l and can be determined from the measured energy and angle of the scattered electron, as usual for deep-inelastic scattering. In general, however, the photon and electron are produced close to the beam pipe. Since tracking inefficiencies are large for small-angle tracks, it may not always be possible to distinguish the electron from the photon. In this case x_l can be determined

from the invariant mass of the electron–photon system $M_{e\gamma}^2 = (l' + k)^2$ since

$$x_M \equiv \frac{M_{e\gamma}^2}{s} = \frac{\hat{s}}{s} = x_l \tag{15}$$

as $Q_h^2 \to 0$. That this is a good approximation is demonstrated by figure 4, which presents a scatter plot of x_l against x_M.

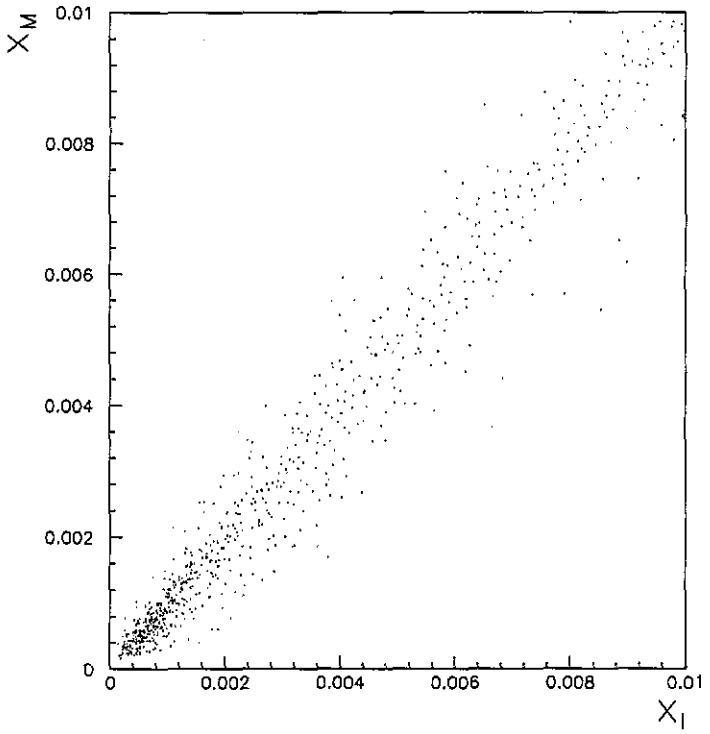

Figure 4. A scatter plot of $x_l = Q_l^2/2p \cdot (l - l')$ and $x_M = M_{e\gamma}^2/s$.

The photon density of the proton $D_{\gamma/p}$ is obtained from the observed x_M distribution of the Compton peak cross section. From (9) and (10) one obtains

$$\left.\frac{d\sigma}{dx_M}\right|^C = \frac{2\pi\alpha^2}{x_M s^2} \int dy_l \frac{1 + (1 - y_l)^2}{1 - y_l} D_{\gamma/p}(x_M, Q_l^2). \tag{16}$$

The photon density can be factored out of the integral by setting $Q_l^2 \approx x_M s$ which corresponds to approximating the density by its value where the cross section peaks, at $y_l = 1$. After the observed x_M distribution has been corrected for the experimental acceptance, it is a simple matter to extract $D_{\gamma/p}$ by dividing by the remaining multiplicative factor. The result is shown in figure 5, where the error bars show the expected statistical errors for an integrated luminosity of $100\,pb^{-1}$. Superimposed is also shown the photon density predicted by (13) using the HMRSB structure function set. The two curves have been normalized to the same number of events in the range $x > 2 \times 10^{-4}$. The two curves are in good agreement except for the lowest-x bins, where the acceptance is poorest. Of course a full unfolding of the photon density is possible with sufficient statistics.

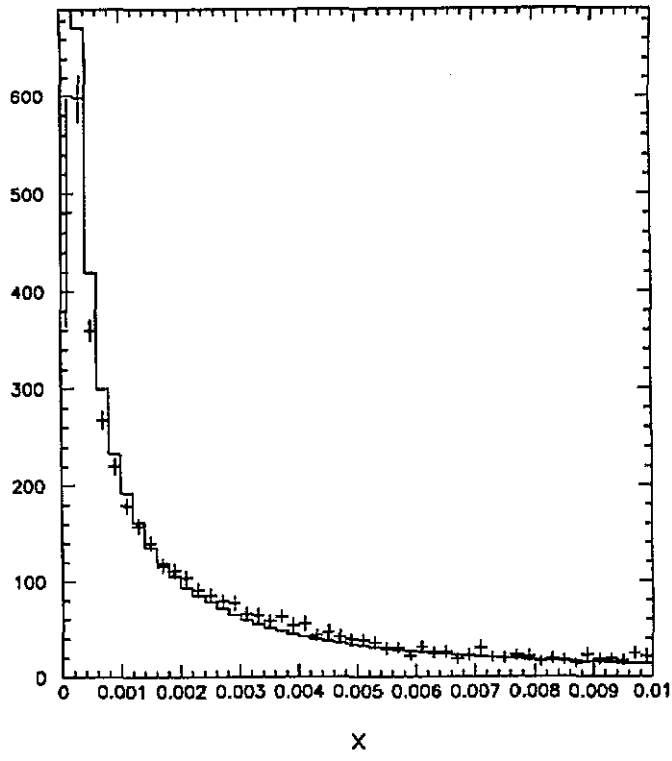

Figure 5. The expected photon density after the extraction procedure described in the text. The errors represent the statistical errors for an integrated luminosity of 100 pb^{-1}. The solid histogram is the prediction of (13) for HMRSB [21]. The units of the vertical scale are arbitrary.

4. Conclusions

Wide-angle radiative scattering is well understood as part of bremsstrahlung processes. As a result, it can be used in an experimental program which seeks to explore the structure of the proton. In this paper we presented formulae for the cross section of the Compton process. From a detailed Monte Carlo study we have suggested how the photon density of the proton may be extracted from HERA data. This information may be used to constrain the low-Q^2 behaviour of F_2 and F_L.

References

[1] Spiesberger H *et al* 1991 *Proc. Workshop Physics at HERA (Hamburg, 1991)* vol 2, ed W Buchmüller and G Ingelman, p 798, and references therein
Böhm M and Spiesberger H 1987 *Nucl. Phys.* B **294** 1081
Bardin D Y, Burdik C, Christova P C and Riemann T 1989 *Z. Phys.* C **42** 679
Spiesberger H 1989 DESY preprint DESY-89-175
[2] Grammer G Jr and Sullivan J D 1978 *Electromagnetic Interactions of Hadrons* vol 2, ed A Donnachie and G Shaw (New York: Plenum) p 195
[3] Aubert J J *et al* (EMC collaboration) 1981 *Z. Phys.* C **10** 101
[4] Aubert J J *et al* (EMC collaboration) 1989 *Phys. Lett.* **218B** 248
[5] Krasny W A, Płaczek W and Spiesberger H 1992 *Z. Phys.* C **53** 687

[6] Beenakker W, Berends F A and van Neerven W L 1989 *Proc. Radiative Corrections for e^+e^- Collisions (Ringberg, 1989)* ed J H Kühn (Berlin: Springer) p 3
[7] Blümlein J 1990 *Z. Phys.* C **47** 89
[8] Kripfganz H, Möhring H-J and Spiesberger H 1991 *Z. Phys.* C **49** 501
[9] Mo L W and Tsai Y S 1969 *Rev. Mod. Phys.* **41** 205
[10] Blümlein J, Levman G and Spiesberger H 1991 *Proc. 1990 Summer Study on High Energy Physics, Research Directions for the Decade (Snowmass, CO)* ed E L Berger (Singapore: World Scientific) p 554
[11] Derrick M *et al* (ZEUS collaboration) 1993 *Phys. Lett.* submitted
[12] Kwiatkowski A, Möhring H J and Spiesberger H 1992 *Comp. Phys. Commun.* **69** 155; 1991 *Proc. Workshop Physics at HERA (Hamburg, 1991)* vol 3, ed W Buchmüller and G Ingelman, p 1294
[13] Courau A, Kermiche S, Carli T and Kessler P 1991 *Proc. Workshop Physics at HERA (Hamburg, 1991)* vol 2, ed W Buchmüller and G Ingelman p 902
[14] Bilenkii S M 1982 *Introduction to the Physics of Electroweak Interactions* (Oxford: Pergamon)
Feynman R P, Kislinger M and Ravndal F 1971 *Phys. Rev.* D **3** 2706
[15] Bardin D, Akhundov A, Kalinovskaya L and Riemann T 1992 *Proc. Zeuthen Workshop on Elementary Particle Theory—Deep Inelastic Scattering (Teupitz, 1992)*
Blümlein J and Riemann T (eds) 1992 *Nucl. Phys.* B (Proc. Suppl.) **29A** 209
[16] Volkonsky N Yu and Prokhorov L V 1975 *Sov. Phys.-JETP Lett.* **21** 389
[17] Martin A, Stirling J and Roberts R 1993 *Phys. Lett.* B **306** 145
[18] Badełek B, Bentvelsen S, Kooijman P, Kwieciński J, Spiesberger H and von Schlippe W 1993 *J. Phys. G: Nucl. Part. Phys.* **19** 1671
[19] Brasse F W *et al* 1976 *Nucl. Phys.* B **110** 413
[20] Stein S *et al* 1975 *Phys. Rev.* D **12** 1884
[21] Harriman P N, Martin A D, Stirling W J and Roberts G G 1990 *Phys. Rev.* D **42** 798
[22] Marchesini G *et al* 1992 *Comp. Phys. Commun.* **67** 465
[23] Caldwell A (ZEUS collaboration) 1992 *Proc. XXVIth Int. Conf. on High Energy Physics (Dallas, 1992)*
[24] Brasse F W (H1 collaboration) 1992 *Proc. XXVIth Int. Conf. on High Energy Physics (Dallas, 1992)*